B. Tannian, N. Goldstein, M. Fox, M. Stark, R. Sundberg, K. Davis and L. Chiemlewski “Flight Testing and Characterization of THIA, a Terrestrial Hyperspectral Imaging Apparatus for Ecological, Agricultural and Mining Applications," Proc. SPIE 12519 Conference: Algorithms, Technologies, and Applications for Multispectral and Hyperspectral Imaging XXIX, (30 April 2023).

DOI: https://doi:10.1117/12.2663813

Paper can be found below.

Flight Testing and Characterization of THIA, a Terrestrial Hyperspectral Imaging Apparatus for Ecological, Agricultural and Mining Applications

B. Tannian*[1], N. Goldstein[1], M. Fox[1], M. Stark[1], R. Sundberg[1], K. Davis[2] and L. Chiemlewski[2]
[1]Spectral Sciences, Inc., 30 Fourth Ave, Burlington, MA, USA 01803; [2] Northrop Grumman Systems Corporation, 1212 Winterson Road, Linthicum, MD 21090

ABSTRACT

The THIA instrument is a visible through extended short-wave infrared (SWIR) imaging spectrometer. Designed using a solid block optical system and a single camera, the sensor is extremely compact with low power requirements. The spectrometer, manufactured by Corning, consists of reflective optical and grating surfaces diamond turned onto a single block of CaF2. The system has been flown repeatedly on a Matrice 600 hexacopter and on small aircraft for data collections. It operates from 0.4-2.45 microns, with high throughput due to the fast f/1.5 optics and has a total weight of 2.4 kg.

THIA SNR was designed to exceed 100 over the full spectral range from 400 to 2450 nanometers under normal operating conditions and exceed 250 below 1700 nanometers. The first prototype system exhibits degraded throughput below 500 nanometers, but meets the SNR threshold over the rest of the range. Stray light backgrounds in the initial prototype require software correction. Despite these issues, the system has been used to obtain meaningful data. Here we characterize THIA Signal-to-Noise in flight conditions and compare results to predicted and benchtop performance.

Keywords: Hyperspectral, Vis/SWIR, UAS, compact, sensor, imaging, remote sensing

1. INTRODUCTION

The THIA (Terrestrial Hyperspectral Imaging Apparatus) sensor, shown in Figure 1, is a new drone-based Hyperspectral Imager (HSI) that covers the full spectral range from 400-2450 nm (Visible through extended Short Wave Infrared or Vis/SWIR) in a compact, ready-to fly package. It was developed by Spectral Sciences Inc., (SSI) in collaboration with Corning Specialty Materials, Advanced Optics Division [1,2], to address the current needs for high resolutions spectral imagery, informative mapping and analytics in the fields of Intelligence, Surveillance and Reconnaissance (ISR) land management, and exploration. THIA extends the availability of the highest quality scientific data to the of intelligence and surveillance community, agribusinesses, researchers in ecology and agronomy, land managers and other businesses in areas such as agriculture, wildfire tracking, climate science. It will be particularly useful for periodic monitoring of high value crops that need detailed, information rich mapping of fields and uncultivated land, collected frequently throughout the growing season.

The THIA design is based on Corning's unique, patented, high-performance solid-block spectrograph technology [3]. The Vis/SWIR sensor is packaged with Corning's existing Shark data acquisition system, in common with their Vis-NIR 410 HSI sensor. Weighing just under 2.4 kg, THIA is light enough to fly on a small, unmanned aircraft like the DJI Matrice-600, as shown in Figure 1. Prototype development was sponsored by the DOE for monitoring of vegetative state and carbon sequestration at the landscape level, but the sensor can be used for a wide range of applications.

In this work, we present a performance evaluation of the THIA HSI imager and present some in-flight data obtained from both a drone and a manned aircraft. Spectral and spatial performance were measured both in the laboratory and in-flight. Drone-mounted HSI data were collected over calibration and resolution targets for calibration purposes, and over agricultural land. We also present data obtained from an aircraft taking survey data at elevations of 10,000-30,000 ft, which demonstrate the utility for landscape-scale monitoring.

*btannian@spectral.com; phone 781 273-4770; fax 781 270-1161; spectral.com

Figure 1. The THIA sensor mounted on DJI Matrice-600 hexa-copter.

2. SENSOR DESIGN AND CALIBRATION

2.1 Sensor design

Figure 2 shows a cutaway view of the THIA sensor. It is a ready-to-fly, self-contained sensor package equipped with a spectrograph, an order sorting filter, a camera to record the optical signal, a control computer with onboard memory, a shutter, an inertial navigation unit that connects to an external GPS antenna, and an f=15mm telescope. The sensor has 680 spatial channels and 410 spectral channels with 4.7 micron spacing. Typical operation is as a pushbroom HSI sensor, operating at a 100 Hz frame rate.

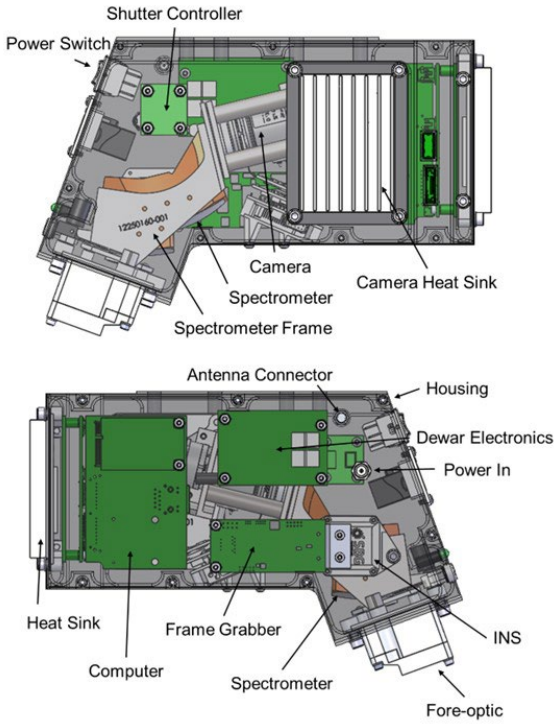

Figure 2. Cutaway view of THIA sensor.

The spectrograph captures one spatial line of scene imagery, disperses each pixel of the line into its spectral components in the direction perpendicular to the slit, and focuses the dispersed light onto a 2D focal plane array (FPA). To acquire a 2D scene, the line of spectrograph imagery is scanned in a push-broom fashion with synchronous framing of the FPA. This can be achieved with constant forward motion of an aircraft, by mechanical rotation or translation of the sensor, or through the use of a scanning input mirror. The data are then geo-registered based on data from an on-board inertial navigation unit.

The spectrometer is an Offner-type design, with gratings and mirrors machined into the solid transmissive calcium fluoride (CaF2) block (Figure 3). The high index material enables an extremely compact design with high numerical aperture (f/1.5) and signal-to-noise. The result is a system covering the 400-2450 nm spectral range with a single foreoptic, spectrograph, and camera. Because the optical surfaces are machined into a single block, they remain in alignment over time and when the block expands and contracts with temperature. Corning's advanced optical machining techniques will allow volume production at low cost.

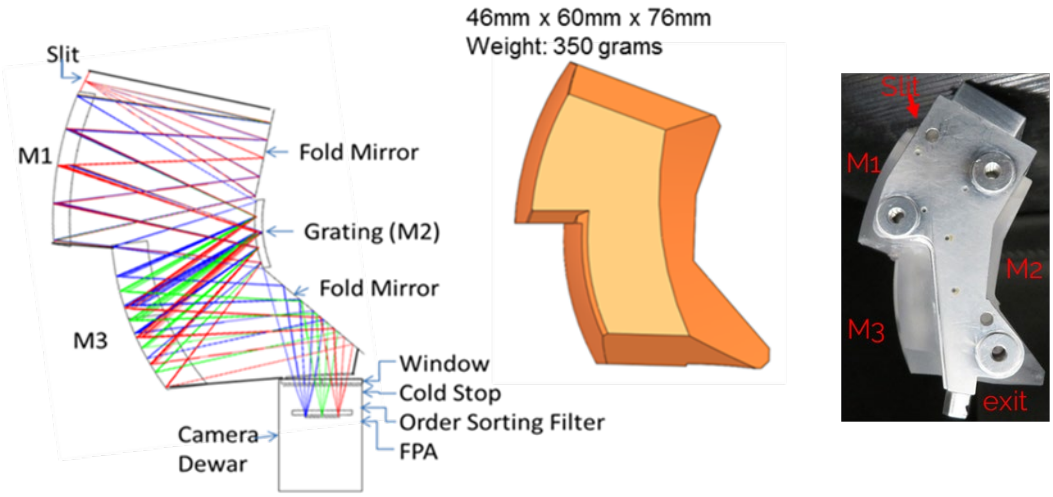

Figure 3. Spectrograph ray trace (left), solid model of the spectrograph block (middle) and a photograph (right) prior to coating.

The optical surfaces, including the grating, are cut and polished directly into the monolith. The powered surfaces, M1, M2, and M3, utilize aspherical optics to provide high spatial and spectral resolution with very high optical throughput. A dual blazed grating is utilized to provide high diffraction efficiency over the 3½ octave spectral range. High-reflection coatings are applied to the optical surfaces, which are then fully encapsulated for environmental immunity. Other processes coat non-optical surfaces with an absorber to eliminate stray light [1,2].

2.2 Spectral calibrations, resolution, and smile

The spectral and spatial performance of the THIA HSI imager were extensively tested in the laboratory and in flight. For spectral calibration in the laboratory, the sensor aperture was overfilled with light from an integration sphere containing Hg and Kr atomic line lamps. Figure 4 shows the resulting dispersed image on the focal plane and the resulting spectral trace at the center top and bottom of the image field. Figure 4 also identifies the three resolved HgAr lines and two resolved Kr lines used for calibration. These atomic line spectra were fit to determine the spectral calibration as a function of spatial position and the spectra line width. Figure 5 shows the results of fitting each of the 640 spatial channels to a gaussian line shape. The overall dispersion is 4.519 nm/channel, and all rows have the same line center within 0.2 spectral channels. Figure 5 shows the characteristic "smile" shape, which varies systematically as a function of wavelength, with a positive sign below 1000nm, and a negative sign above 1000nm. In all cases, the smile is less than 0.2 pixels or 0.9 nm. This near-uniformity in spectral calibration across the spatial field allows for direct comparison of spectra obtained anywhere within the image field.

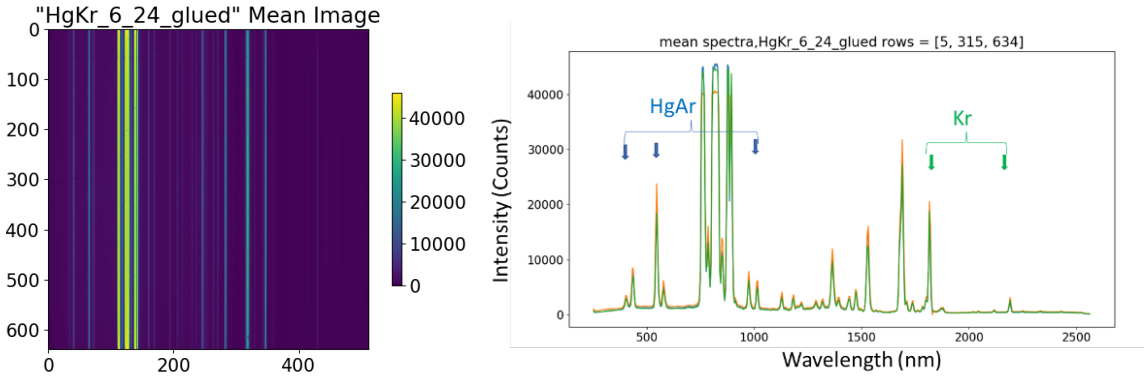

Figure 4. Spatial Calibration with line lamps. Right- dispersed image. Left- Spectra indicating lines used for the spectral calibration.

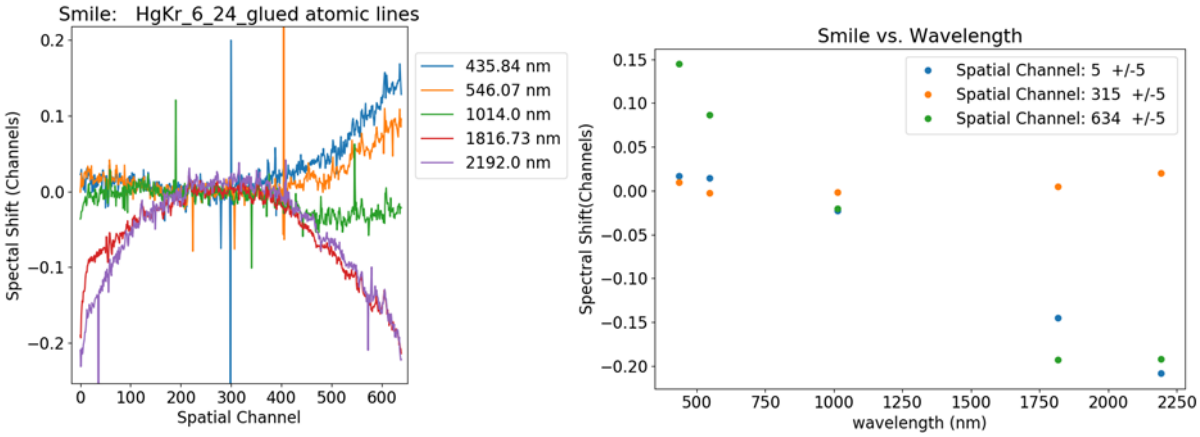

Figure 5. Spectral shift as function of spectral channel (left) and wavelength (right).

Figure 6 shows the measured spectral line width obtained from the fit to a Gaussian line shape. The line width, as measured by the Full Width Half Maximum (FWHM), ranges between 2.1-2.4 spectral channels or 9-11nm. It is uniform over the spatial field and has a small dependence on wavelength with the widest peaks in the blue-green spectral region.

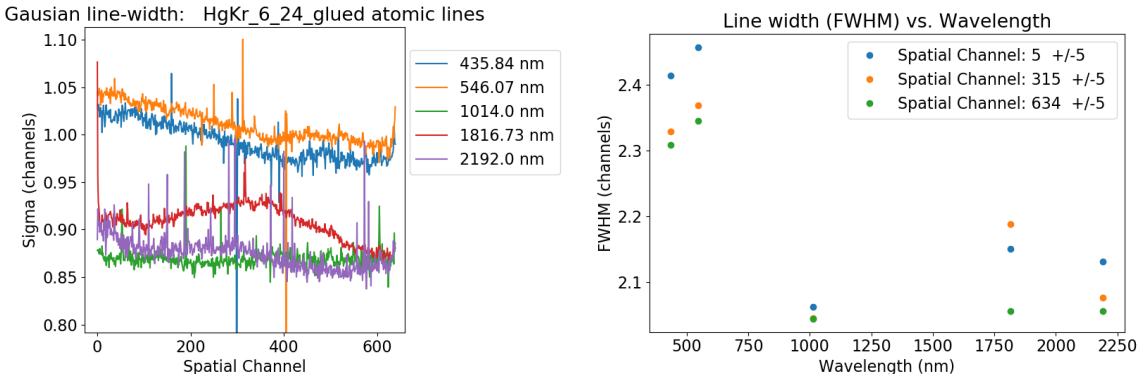

Figure 6. Measured line width for each spectral channel (left) and as function of wavelength (right).

3. IN-FLIGHT MEASUREMENTS OF SNR AND SPATIAL RESOLUTION

The sensor spatial resolution and signal to noise ratio were tested by flying over a set of overlapping Permaflect reflectance panels at an altitude of 25 m, to produce hypercubes. Figure 7 shows a single-color image of the panels at 1012 nm, with the three calibration panels at the left-hand edge.

The spectrally resolved average output of the sensor for the nominal 40% and 80% panels, in radiance units, is shown in left-hand side of Figure 8.

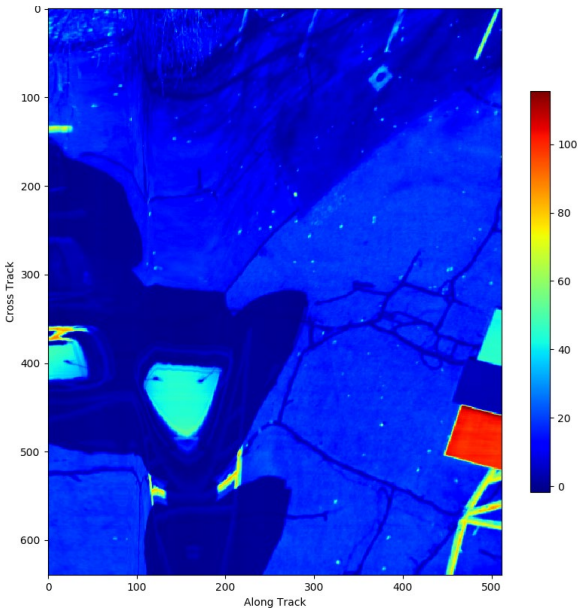

Figure 7. Single color image at 1012 nm showing overlapping Permaflect panels on the right-hand edge.

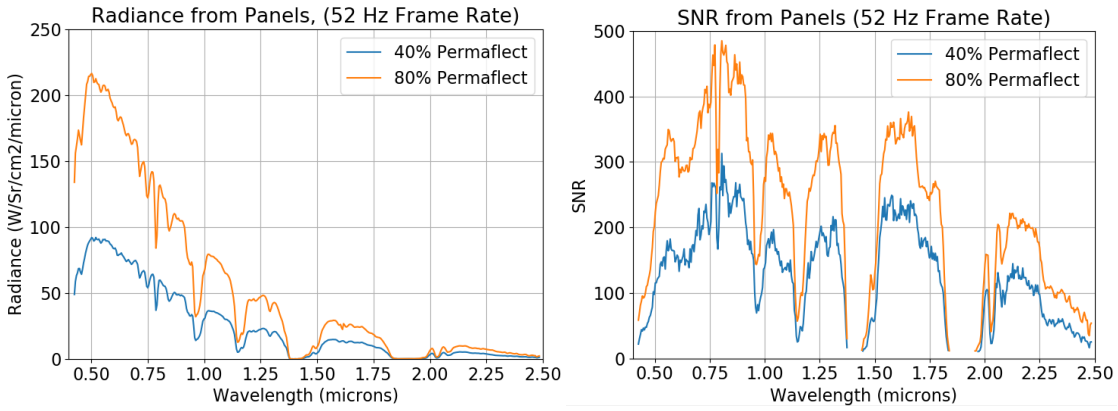

Figure 8. Average radiance (left) and SNR (right) for nominal 40% and 80% Permaflect panels.

3.1 In-Flight SNR

The right-hand-side of Figure 8 shows the average Signal-to Noise Ratio (SNR) for each panel which is calculated along track for each of the rows of the image. In doing so, the individual spectral channels were first normalized to the total panchromatic signal to remove trends due to varying surface reflectance across the rows. The results for each row were then averaged to give a characteristic value for the sensor as a function of wavelength, which is typically well above 100:1. The SNR values are within 20% of the values calculated for the sensor, based on the known sensor transmittance, gain, and noise characteristics. For most of the spectral range, the SNR is given by the shot noise on the received photosignals, but the detector read noise and dark current make significant contributions in the weaker bands and are dominant in the center of the water bands and at the edges of the spectral range. In general, anything above SNR=50 is

shot-noise limited; below that, the SNR is read-noise and dark noise limited. The SNR increases with increasing reflectance, solar illumination, and exposure time.

3.2 In-flight spatial resolution measurement

The data of Figure 6 were used to calculate the spatial resolution using the slanted-edge method [4]. A 5% reflective panel was placed on top of the two bright panels to form two edges. The sensor was flown across the panels at a near-constant velocity of about 0.70 m/s, which results in a nearly square aspect ratio in the image; the motion across the slit is equal to 14 microns in the image plane, which is nearly comparable to the 15-micron slit width. Figure 9 through Figure 12 illustrate the measurement of spatial resolution in both the cross-track and along-track directions. In each case, a region of interest (ROI) is designated that crosses the edge in the appropriate direction. The data within the ROI is then up-sampled and projected to align along the direction of the intensity gradient. The image-angle used in the projection was 74.4 degrees for the cross-slit ROI, and 13.4 degrees for the along-track ROI. (While the two angles should nominally add to 90 degrees, they do not quite, due to rotation of the sensor in between measuring the two ROI.)

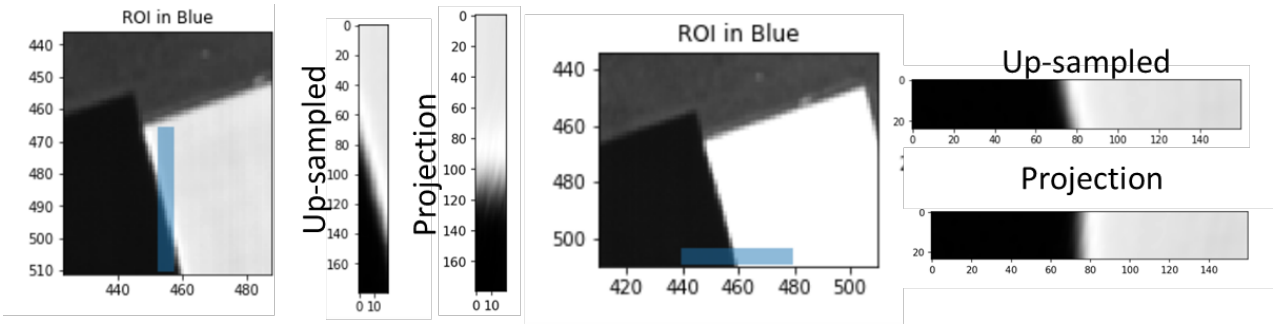

Figure 9. Regions of Interest (ROI) shown in blue and up-sampled data before and after projection along the gradient for cross-track (left) and along-track (right) measurements.

Figure 10 through Figure 12 show the extraction the Edge Spread Function (ESF), Line Spread function (LSF) and Modulation Transfer Function (MTF) for each ROI. First, the ESF is calculated for each of the rows or columns of the up-sampled, projected image and averaged to form a single ESF for all the columns, as shown in the Figure 10 for one wavelength of 1631nm. The left-hand side shows the cross-track ESF and the right-hand side shows the along-track ESF. The Line Spread Functions (LSF), shown in Figure 11, is formed by differentiating the ESFs. It plots the LSF in both directions for six wavelengths that span the spectral range. Finally, the Modulation Transfer Functions (MTF), shown in Figure 12, are calculated as the Fourier Transform of the LSF functions.

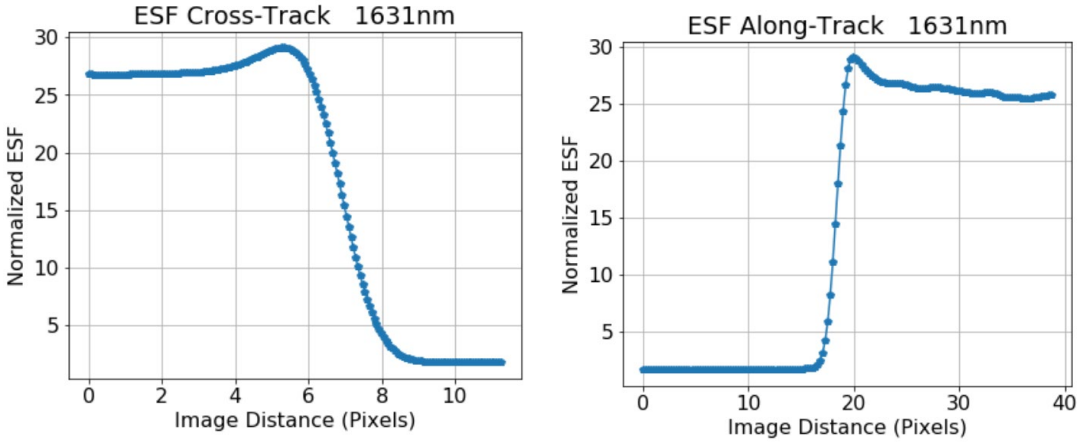

Figure 10. Averaged ESF for the Cross-Track (left) and Along-Track (right) directions.

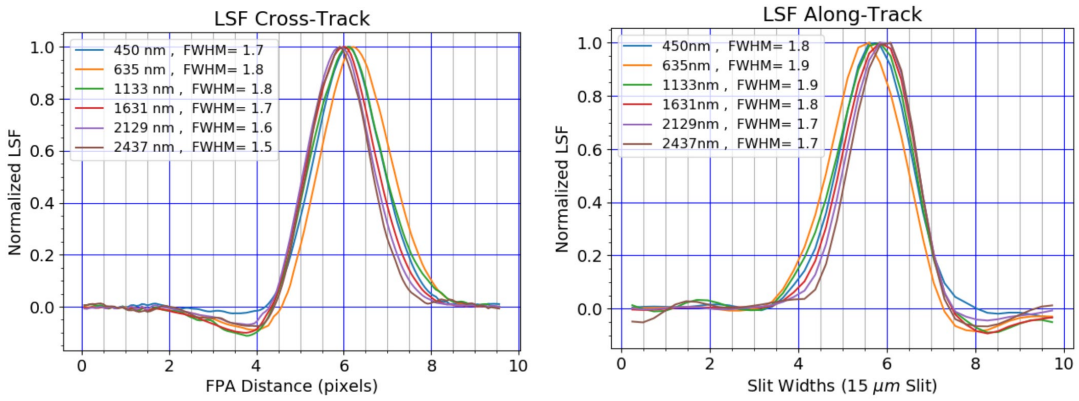

Figure 11. Line Spread Functions (LSF) for the Cross-Track (left) and Along-Track (right) directions.

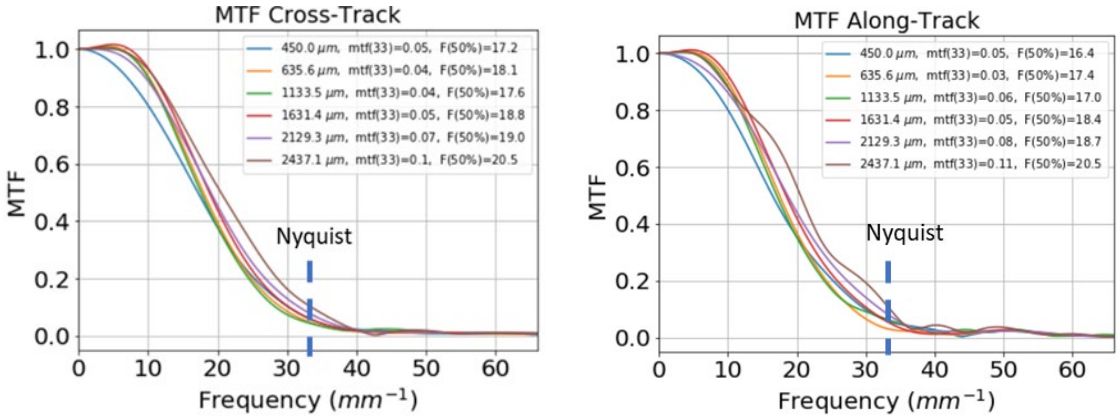

Figure 12. Modulation Transfer Functions (MTF) for the Cross-Track (left) and Along-Track (right) directions.

The spatial Full Width Half Maxima (FWHM) for each wavelength are also reported in Figure 11. They are similar across both directions, and all spectral bands, with Full Width Half Maxima from 1.5–1.9 pixels. The line centers are coincident within experimental error (0.2 pixels), indicating minimal effects of slit rotation, smile and keystone. This verifies the laboratory measurement of these quantities as shown above. The close coincidence of the spatial features for all spectral lines is a necessary condition for the analysis of hyperspectral images, as a shift in spatial position with wavelength would result in mixing of spectra across adjacent pixels. Figure 13 lists the MTF values at the Nyquist sampling frequency of 33 line pairs/mm, and the frequency at which the MTF is equal to 50%, which is typically about 18-20 line pairs/mm. These values are in good agreement with the FWHM values. The spatial resolution, as measured in the LSF and MTF functions, is affected by astigmatism in this, the first copy of the spectrograph. Laboratory measurements prior to assembly, showed significantly higher spatial resolution for both the telescope and spectrograph, but there was a focal shift between the tangential and sagittal foci. The telescope was therefore aligned to achieve a compromise at the circle of least confusion. This astigmatism has been improved in subsequent iterations of the spectrograph through improvements in machining metrology. But even prior to those improvements, the spatial resolution of FWHM≈1.8 channels provides very good spatial resolution; it is well matched to the spatial-channel density to provide critical sampling of the line-spread function.

4. FLIGHT DATA

SSI has performed preliminary drone test-flights at local sites, including farm plots at Soule Homestead Education Center in Middleborough, MA. Scenes of trees, grass, late-season crops, and manmade objects were captured at altitudes ranging from 10m to 120m. Raw data collected by the sensor includes hyperspectral data cubes, dark frames acquired at the start and end of each flight pass, and input geometry data (IGM) files containing the latitude and longitude of each pixel in each frame. These data cubes were processed to radiance by applying the sensor calibration values and then to reflectance using QUAC [5] for atmospheric correction.

An example of the use of THIA data for plant phenotyping appears in Figure 13. The left side shows an RGB representation of a data cube from a 25m altitude flight over a partially harvested field. We selected a spectrum from one of the plants in the middle row and used an Orthogonal Subspace Projection (OSP) [6] to find other instances of the plant. The white pixels on the right represent matches to that plant spectrum above a threshold value.

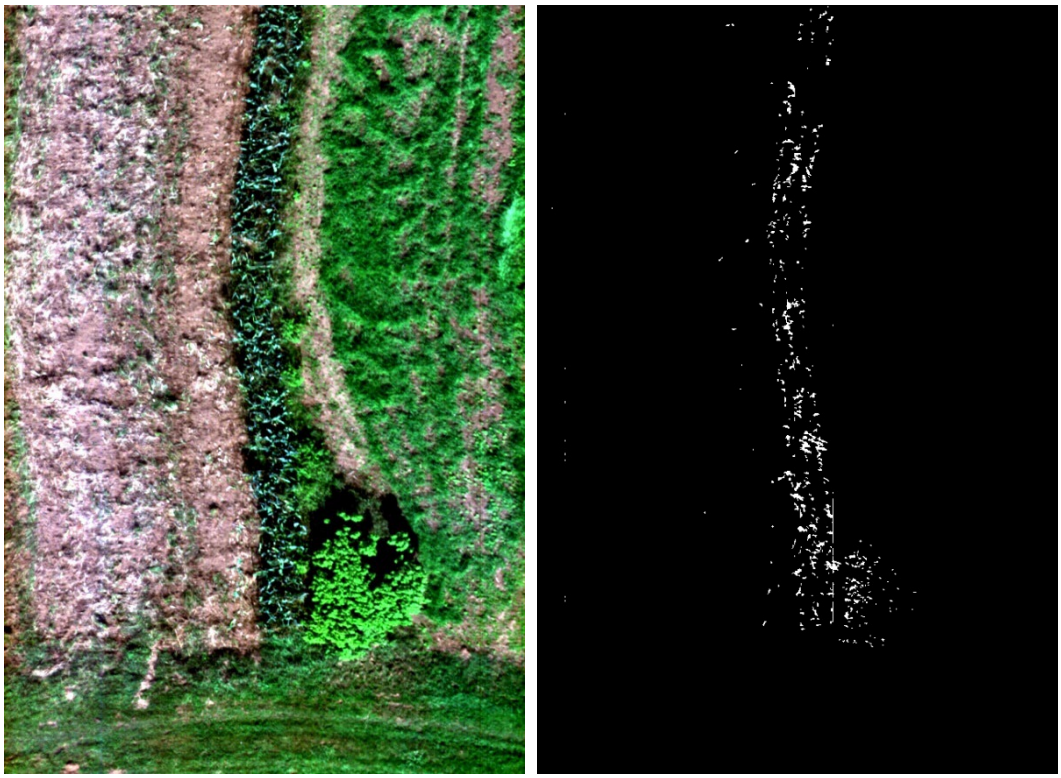

Figure 13. Plant phenotyping using the THIA sensor.

Figure 14 shows a larger swath of the farm imaged from an altitude of 120m. In addition to plants and soil, this scene contains calibrated Permaflect panels and a number of manmade objects, including a tractor and some plastic bins. We identified other plastic bins in the scene based on the average spectrum of a small region of interest in the middle of the white plastic bin lid about halfway across the image and about 1/3 of the way from the bottom. Other plastic materials were identified using Adaptive Cosine Estimation (ACE) algorithm [7] which returns a score between 0 and 1 based on the overlap of the spectra. The ACE scores are shown graphically in the center and right panels of Figure 14. Results for the white plastic are shown using either the full vis/SWIR spectrum, or just the vis/NIR spectrum typical of most visible HSI sensors. The center panel uses the full vis/SWIR spectrum acquired by the sensor. The right panel uses only the spectral range commonly available for compact sensors, 400-1100 nm. In both cases, the ACE score is easily able to distinguish between the plants and soil and the selected plastic lid. When using only the visible region though, many other manmade materials, including painted surfaces and other types of plastic, result in a false positive ace score to that of the bin lid. However, these false positives are eliminated when including the full spectral range of 400-2450 nm. ROC curves for the detection of the same plastic lid for the two spectral ranges appear in Figure 15. False detections are significantly more common in the visible-only case, indicating that data from the SWIR bands are helpful in discriminating this material.

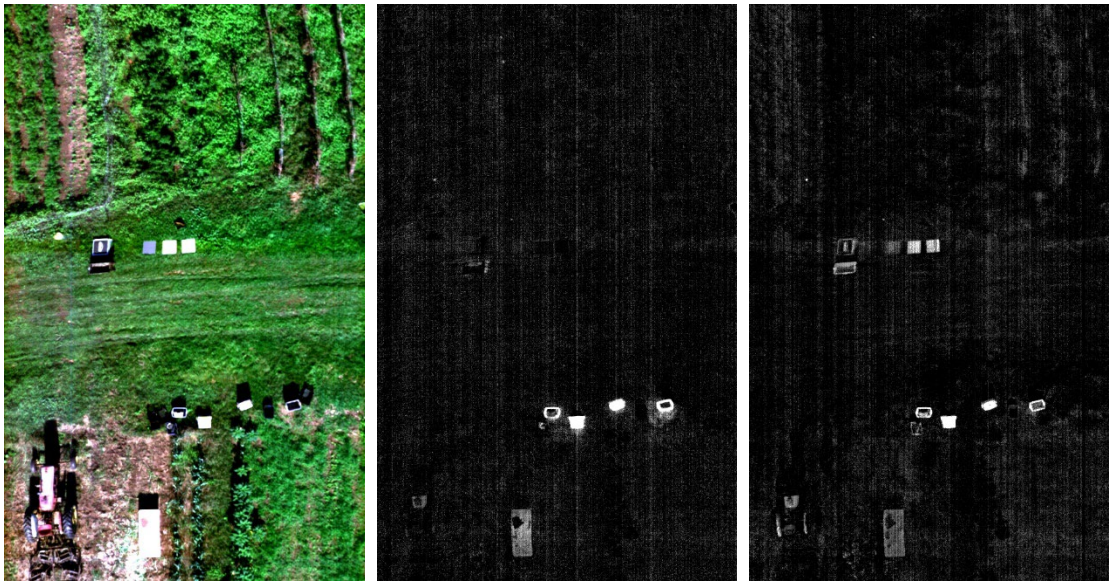

Figure 14. We chose the white plastic lid and mapped ACE scores to match. Center: Full spectrum ACE scores. Right: Spectral range cut off at 1100 nm.

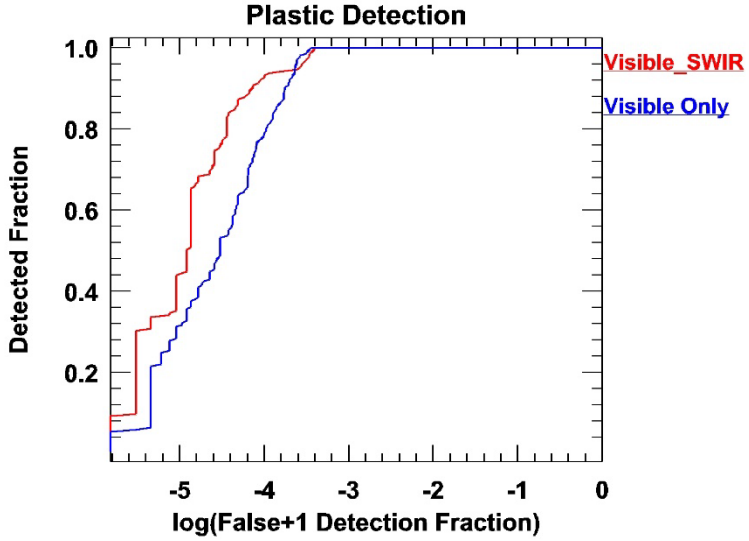

Figure 15. ROC curves for detection of the matches to the plastic lid with varying ACE threshold.

Another series of data collects were conducted in collaboration with Northrop Grumman's HOP Queue (Hyperspectral Onboard Processing Queue) demonstration project [8]. This allowed for the THIA instrument to be integrated into the belly of a manned aircraft to collect data throughout the Chesapeake Bay area and the Great Dismal Swamp in Virginia, with the primary goal of measuring the health of the coastal waters and forests in these regions. Additional data was taken over a series of ground tarps for calibration purposes. Flights were conducted at around 5000 feet above sea level and varying frame rates.

In Figure 16, we show a section of the swamp near the Virginia/North Carolina border. The left-hand side shows a radiometrically calibrated RGB image as recorded by the sensor. The middle image shows the same image after geo-registration using the IGM files. The color scale has been stretched to emphasize contrast in the green. The right-hand side shows the same area as seen in google maps. The curvature of the top and bottom of the geo-registered image reflect the curvature of the sensor image field. The wiggly edges at the sides, reflect the variation in airplane and sensor pointing during flight.

These data were collected at an altitude of 1700 meters above ground level, thus giving a ground sampling distance of about 1.6 meters. In this scene, there are several different types of vegetation, dirt, road, and water features. In Figure 17, we show representative spectral signatures for various types of vegetation, roads, canal water, and bright clouds. Using these spectra, we performed a series of Orthogonal Subspace Projection (OSP) calculations to identify the different spectral features in the scene [6]. The OSP detection map for Kudzu, a perennial plant invasive to the region, two additional types of crops (labeled A and B) and the road are shown in Figure 18 from left to right, respectively.

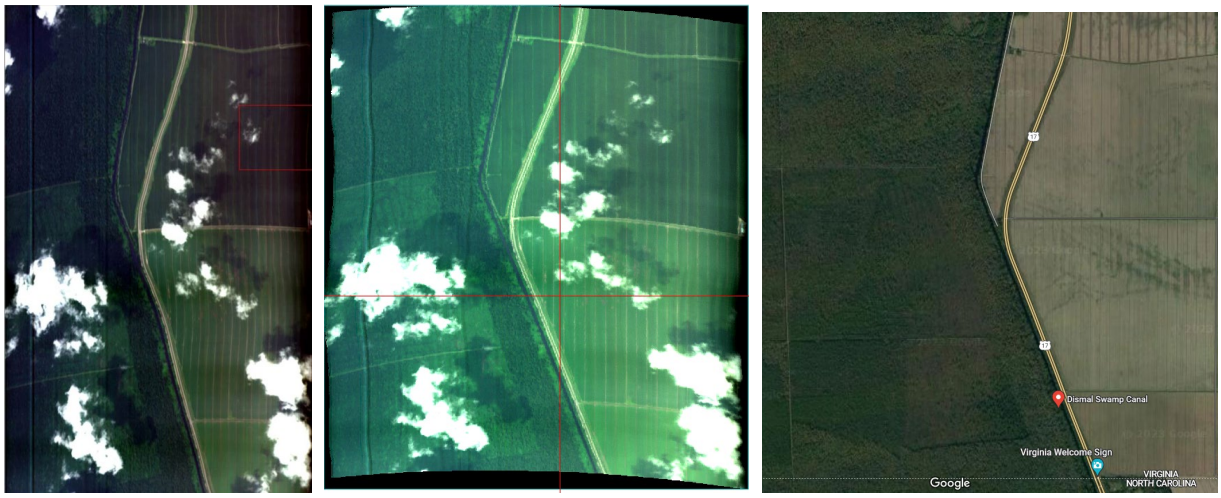

Figure 16. Images of the Great Dismal Swamp. DGB image before (left) and after geo-rectification (middle) compared to google maps) (right).

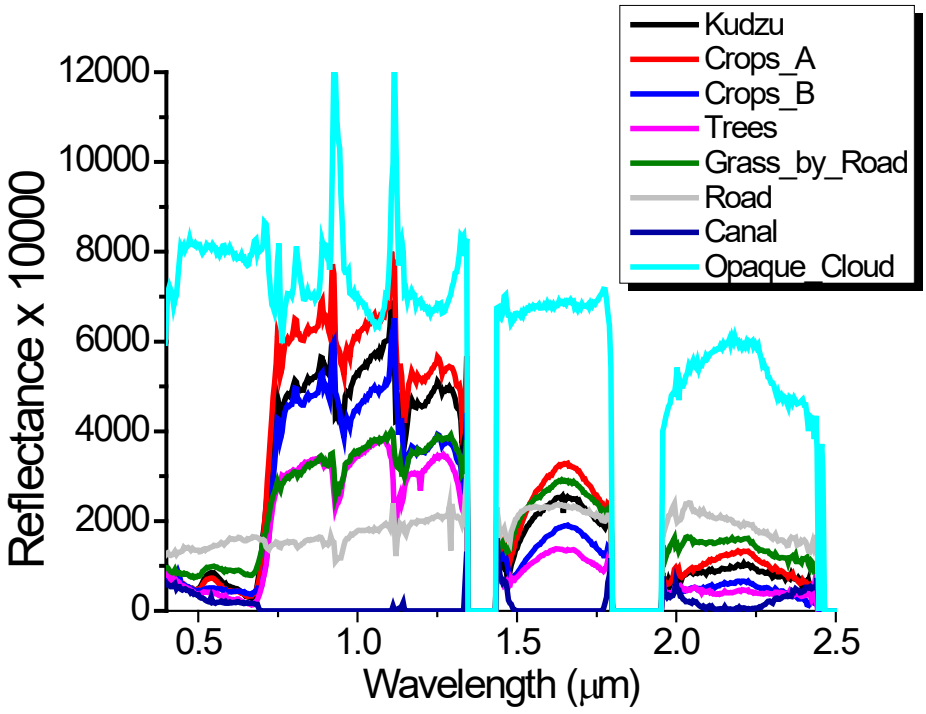

Figure 17. Spectra for materials selected from the THIA collect shown in Figure 16.

Figure 18. OSP detection maps for Kudzu, Crop A, Crop B and the road, left to right.

5. CONCLUSIONS

We present a compact, ready-to-fly vis/SWIR hyperspectral package based on a monolithic Offner spectrograph machined from solid CaF2. The THIA sensor covers the full spectral range of 400-2450 nm with a single spectrograph and a single HgCdTe FPA. It includes an f=15 mm telescope and all necessary electronics in a package weighing less than 2.4 kg that can be flown on a variety of class 1 UAVs. The sensor has 680 spatial channels spatial resolution, and 410 spectral channels with 4.7 micron spacing. Typical operation is as a pushbroom HSI sensor, operating at a 100 Hz frame rate.

Extensive testing of spatial and spectral resolution shows critical sampling of the spatial and spectral data with spatial resolution of FWHM≈1.8 spatial channels and Spectral resolution of FWHM<10nm or 2 spectral channels. Smile and keystone are minimal, with smile < 0.2 spectral channels. SNR is greater than 100:1 throughout most of the spectral range.

The full sensor package has been demonstrated in test flights with a hexacopter drone and in a manned aircraft. Initial applications will be in vegetative status monitoring in support of DOE ecology research. Other applications include agriculture, mineralogy, and ISR.

6. ACKNOWLEDGEMENTS

The authors gratefully acknowledge the financial support from DOE under SBIR Contact No. DE-SC0015126, Daniel Stover Program Manager, and the advice and collaboration of Sean Serbin of DOE Brookhaven National Laboratories in defining future measurement campaigns.

REFERENCES

[1] Ziph-Schatzberg, L., Wiggins, R., Woodman, P., Saleh, M., Nakanishi, K, Soletsky, P., Goldstein, N., Fox, M., Tannian, B., “Compact visible to extended-SWIR hyperspectral sensor for Unmanned Aircraft Systems”, Proc. SPIE 10644, (2018)

[2] Goldstein, N., et. al. “Fabrication and testing of a UAS-based visible to extended-SWIR hyperspectral sensor,” WHISPERS 2019.

[3] Ziph-Schatzberg L., Woodman P., Nakanishi K., Cornell J., Wiggins R., Swartz B., and Holasek R., “Compact, high performance hyperspectral systems design and applications,” SPIE Defense, security and sensing. p. (94820W) (April 2015)

[4] Haefner, D., "MTF measurements, identifying bias, and estimating uncertainty", in Infrared Imaging Systems: Design, Analysis, Modeling, and Testing XXIX, Keith A. Krapels; Gerald C. Holst, Editors, Proceedings of SPIE Vol. 10625 (SPIE, Bellingham, WA 2018), 1062506.

[5] Bernstein, L.S., X. Jin, B. Gregor and S.M. Adler-Golden, “Quick atmospheric correction code: algorithm description and recent upgrades,” Opt. Eng. 51(11), 111719 (2012).
[6] Chang, Chein-I. "Orthogonal subspace projection (OSP) revisited: A comprehensive study and analysis." IEEE transactions on geoscience and remote sensing 43, no. 3 (2005): 502-518.
[7] Kraut, S.S., L.L. Scharf, R.W. Butler, “The Adaptive Coherence Estimator: A Uniformly Most-Powerful Invariant Adaptive Detection Statistic,” IEEE Trans. Signal Processing, Vol. 53, No. 2 (2005).
Davis, K., Kher, A., Biddlecomb, J. et al. “n